Advanced Steel Construction – Vol. 22 No. 4 (2026) 407–417
DOI:10.18057/IJASC.2026.22.4.5

ECCENTRIC COMPRESSION MECHANICAL PROPERTIES OF CONCRETE-FILLED SQUARE STEEL TUBE UNDER CORROSIVE PITTING

Wen-Yu Hou [1, 2, *], Di Wang [1] and Ni Zhang [3]

[1] *School of Transportation and Geomatics Engineering, Shenyang Jianzhu University, Shenyang 110168, China*
[2] *Shenyang Key Laboratory of low-carbon Transportation Construction*
[3] *School of Civil Engineering, Liaoning Technical University, 125105, China*
* *(Corresponding author: E-mail: houwenyu61@163.com)*

A B S T R A C T

This paper studies the eccentric compression of short concrete-filled square steel tube column under corrosive pitting. The random pitting is implemented in Python and the short concrete-filled square steel tube column is simulated by the finite element software ABAQUS. The results show that pitting will affect the ultimate bearing capacity of the specimen. The ultimate load of specimens with regular pitting is higher than that of specimens with random pitting. The pitting will reduce the strength of the steel tube, leading to the decrease of the longitudinal stress of the steel tube. Pitting will cause the early contact between steel tube and concrete, reducing the interaction between steel tube and concrete, and causing the reduction of the bearing capacity of the specimen. For every 0.25 increase in eccentricity, the bearing capacity will decrease by approximately 20%. As the strength of the concrete increases, the bearing capacity of the regular pitting specimens is much higher than that of the random pitting specimens, approximately by about 5%. For every 1mm increase in the thickness of the steel tube, the bearing capacity can be enhanced by approximately 8%. Increasing the strength of concrete, the strength of steel tube, and the thickness of steel tube, the bearing capacity of the regular pitting specimens is generally higher than that of the random pitting specimens.

A R T I C L E H I S T O R Y

Received: 15 June 2025
Revised: 9 January 2026
Accepted: 12 January 2026

K E Y W O R D S

Corrosive pitting;
CFST;
Random pitting;
Regular pitting;
Finite element analysis

1. Introduction

Corrosive pitting is a common metal corrosion, as shown in Fig.1. The metal loss caused by the pitting is very small, but it can cause a serious decline in the performance and structural strength of the steel, or even the sudden destruction of the structure[1-3]. The occurrence of pitting corrosion in concrete-filled steel tubular (CFST) structures results in the deterioration of structural stiffness and bearing capacity, as well as a reduction in the service life of the structures.[4-6].

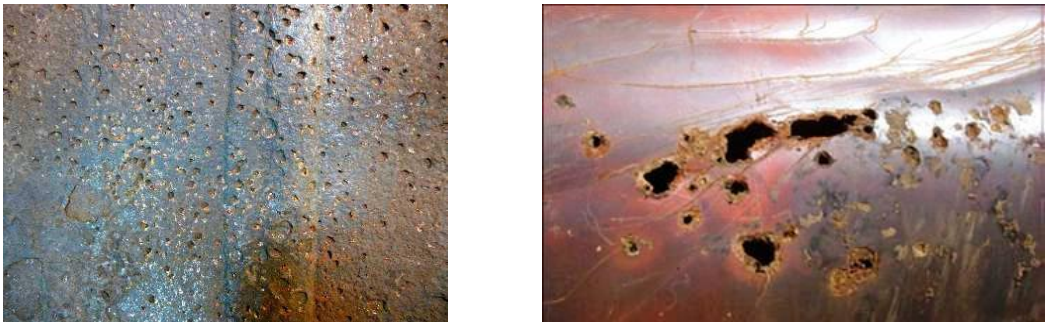

Fig. 1 Metal pitting corrosion

Many experts have studied the mechanical behavior of CFST structures after corrosion[7-10]. Xie[11] *et al*. performed to examine how the acid rain corrosive environment influences mechanical properties of concrete-filled steel tubular (CFST) members. The results indicated that corrosion significantly decreased the yield strength, elastic modulus, and tensile strain capacity of steel plates, along with a notable decline in the ultimate strength of CFST members. Hua[12] *et al*. conducted finite element analysis on concrete-filled steel tubular (CFST) columns subjected to the combined influence of sustained loading and corrosion. The study revealed that sustained loading causes concrete stress hysteresis and alters the strength. Zhang[13] *et al*. investigated the effects of acid precipitation corrosion and freeze-thaw cycles on the degradation of the axial properties of concrete-filled square and thin-walled steel tube. The results showed that acid rain corrosion had more serious effects on stiffness, ductility, confinement effects and ultimate bearing capacity than freeze-thaw. Ali[14] *et al*. tested 11 long concrete-filled square steel tube columns under uniaxial eccentric loading and examined the impacts of concrete strength, slenderness ratio, and eccentricity on parameters like buckling mode and ductility. The findings showed that the type of failure behavior of the eccentric members with high slenderness ratio was overall buckling, starting with yielding of the outer steel tube followed by cracking of the concrete on that side; the ultimate strength of the eccentric members decreased with increasing slenderness ratio and eccentricity. Hui[15] *et al*. performed uniaxial axial compression tests on 15 concrete-filled steel tube columns with varying concrete strengths and corrosion levels to evaluate corrosion's impact on their axial compressive properties. The study revealed that corrosion diminished the characteristics of concrete-filled steel tubular (CFST) members. However, increasing the steel tube's wall thickness can sustain high ductility and stiffness, thereby counteracting corrosion's adverse effects on the structure. Wang[16] *et al*. established a numerical model for concrete-filled locally corroded steel tube to study the effects of corrosion position, corrosion volume rate, and corrosion area rate on the bearing capacity under eccentric loading. When the corrosion volume rate was identical, the bearing capacity of the specimen with mid-span corrosion was found to be lower than that of the specimen with end corrosion. Luo[17] *et al*. introduced an artificially processed defect to simulate the localized corrosion on the surface of steel tube, and tested 45 CFST long columns, medium-length columns, and other columns with different slenderness ratios by different corrosion locations, corrosion volume, corrosion area, and corrosion wall thickness. The results indicated that all specimens' failure modes manifested as overall compressive-bending failure accompanied by localized outward buckling. As the corrosion volume loss increased, the load-bearing capacity, stiffness, and ductility of CFST specimens with localized corrosion decreased to different extents.

In conclusion, the current research on corroded concrete-filled steel tube mainly focuses on concrete filled circular steel tube. The research on concrete-filled square steel tube is relatively scarce. However, in real life, the usage rate of concrete-filled square steel tube is no less than that of circular ones. Moreover, the research on concrete-filled steel tube affected by pitting corrosion is even more scarce. In this paper, the regular and random pitting is implemented in Python and the short square CFST column is simulated by the finite element software ABAQUS. The load-deflection, stress distribution and interaction between different specimens under regular and random pitting are analyzed. The impacts of various parameters on mechanical properties under regular and random pitting are taken into account.

2. Constitutive model of materials

2.1. Steel tube

Based on the data in Fig.2, The elastoplastic mechanical behavior of steel tube has the same properties under tension and compression and the stress-strain relationship is:

$$\sigma=\begin{cases} E_t\varepsilon_t & (\varepsilon_t\le\varepsilon_{te}) \\ -A\varepsilon_t^2+B\varepsilon_t+C & (\varepsilon_{te}<\varepsilon_t\le\varepsilon_{te1}) \\ f_{ty} & (\varepsilon_{te1}<\varepsilon_t\le\varepsilon_{te2}) \\ f_{ty}\left[1+0.6\dfrac{\varepsilon_t-\varepsilon_{e2}}{\varepsilon_{e3}-\varepsilon_{e2}}\right] & (\varepsilon_{te2}<\varepsilon_t\le\varepsilon_{te3}) \\ 1.6f_{ty} & (\varepsilon_t>\varepsilon_{te3}) \end{cases} \tag{1}$$

The variables in the equation are as follows: $A=\dfrac{0.2f_{ty}}{(\varepsilon_{te1}-\varepsilon)^2}$, $B=2A\varepsilon_{te1}$, $C=0.8f_{ty}+A(\varepsilon_{te})^2-B\varepsilon_{te}$, $\varepsilon_{te}=0.8f_{ty}/E_t$, $\varepsilon_{te1}=1.5\varepsilon_{te}$, $\varepsilon_{te2}=10\varepsilon_{te}$, $\varepsilon_{te3}=100\varepsilon_{te}$, E_t is the steel's elastic modulus, f_{ty} is the steel's yield strength, f_{tu} is the steel's ultimate strength.

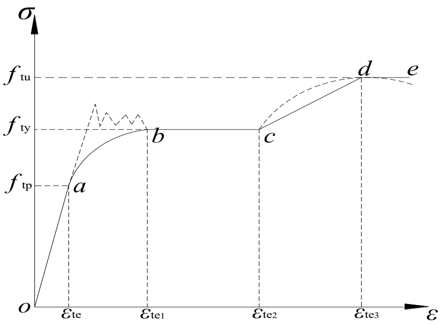

Fig. 2 Steel's stress-strain relationship

2.2. Concrete

The damage model is applied to the concrete, as illustrated in Fig.3, and the stress-strain relationship is:

$$\left.\begin{array}{ll} x\le 1 & y=\alpha_a x+(3-2\alpha_a)x^2+(\alpha_a-2)x^3 \\ x>1 & y=\dfrac{x}{\alpha_d(x-1)^2+x} \end{array}\right\} \tag{2}$$

Where $y=\sigma/f_c$, $x=\varepsilon/\varepsilon_c$, f_c、ε_c are uniaxial compressive strength and peak compressive strain of concrete, $\varepsilon_c=\left(700+172\sqrt{f_c}\right)\times10^{-6}$, $\alpha_a=2.4-0.0125f_c$, $\alpha_d=0.157f_c^{0.785}-0.905$, $\varepsilon_{cu}=\varepsilon_c\left(1+2\alpha_d+\sqrt{1+4\alpha_d}\right)/2\alpha_d$。

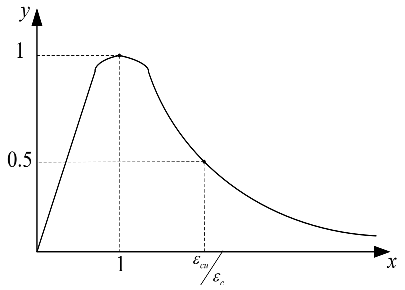

Fig. 3 stress-strain curve of concrete

3. Trial-based validation of the finite element model

The computational simulation results are verified with the test data according to the reference[18].

3.1. Failure pattern of specimen

The failure pattern of the specimen as depicted in the finite element analysis is illustrated in Figure 4. A0-a denotes the uncorroded specimen, whose failure mode is characterized by local bulging in the mid-section of the steel tube and its crushing behavior of the concrete in the compression zone. The failure pattern of specimen A3-O20-A is marked by outward bulging of the steel tube's compression area within the corrosion region, accompanied by lateral bending deformation in the same area.The maximum deflection occurs in junction of the corroded area and uncorroded area, and near the corrosion side. And the steel tube at the junction shows different degrees of buckling. The failure mode of A3-M20-a is the overall lateral bending in the middle section, and the maximum deflection is similar to that of the uncorroded specimen. It occurs in the middle area of the specimen, and the steel tube at the junction of the corroded area on both sides shows different degrees of bulging. The failure mode of A3-B20-a is lateral bending deformation at both ends of the corrosion area, and these deformation are distributed at both ends of the specimen in a symmetrical way. In the junction of the corroded area, the steel tube shows different degrees of buckling, and the concrete within the corrosion affected zone at the junction is crushed.

(a) A0-a (b) A3-O20-a

(c) A3-M20-a

(d) A3-B20-a

Fig. 4 Comparison of failure modes between test and finite element model

3.2. Load-deflection curve

Fig.5 presents the load-deflection curves obtained from tests and finite element analysis. The difference of the ultimate bearing capacity of the specimen is 8.4kN, 1.0kN and 10.6kN, and the deformation difference of the middle section is 0.28mm, 1.09mm and 0mm. The finite element simulation agrees well with the test.

3.3. Load-longitudinal strain curve test

Fig.6 illustrates the load-longitudinal strain curves from both the test and finite element analysis. A high degree of consistency is observed between the test and finite element results for each specimen in the elastic and elastoplastic stages, with an overall consistent trend, confirming the feasibility of the modeling approach.

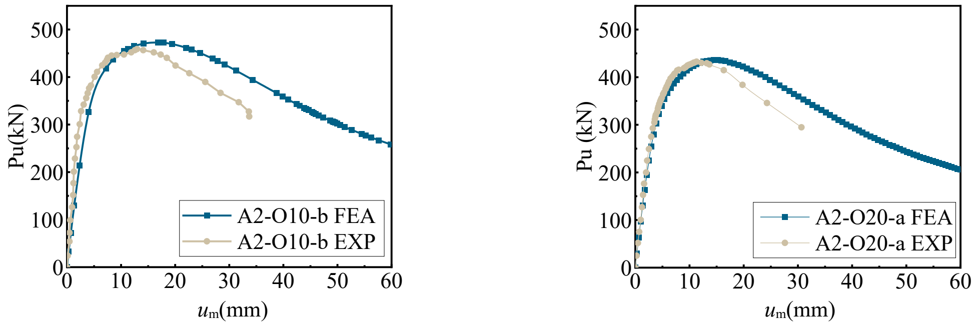

(a) Local corrosion at one end load-displacement curve

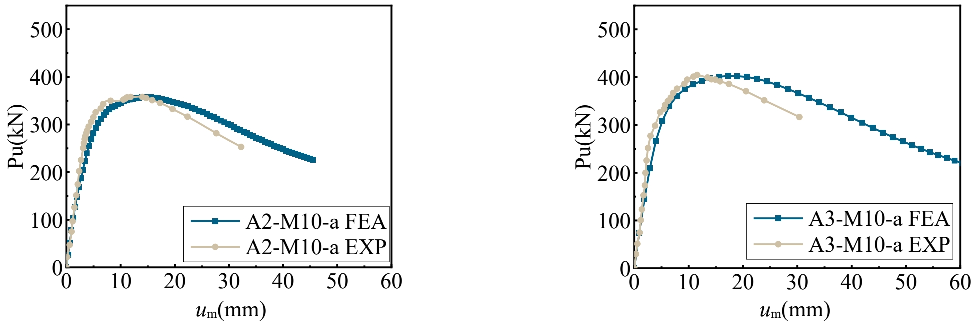

(b) load-displacement curve in the middle of local corrosion

Fig. 5 Comparison of load-displacement curves

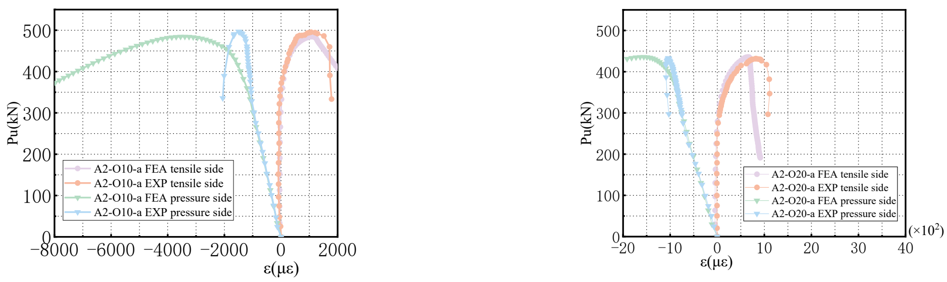

(a) Local corrosion end load-strain curve

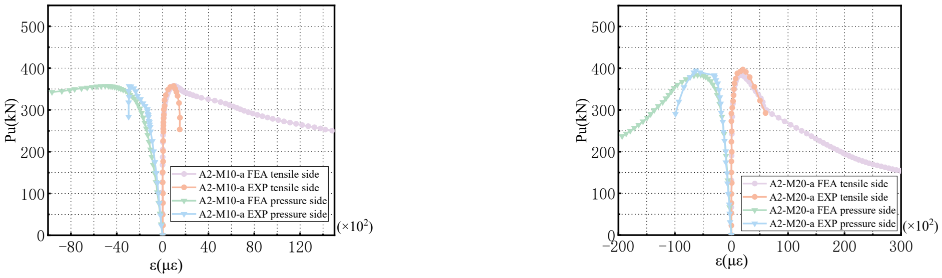

(b) Local corrosion central load-strain curve

Fig. 6 Load-strain curve comparison

4. Realization of the random distribution of pitting

4.1. Shape and distribution of pitting

Because ABAQUS can't directly realize the random distribution of steel tube pitting, the 'RAND function' with the help of 'Python' is used to realize the secondary development of ABAQUS finite elements and complete the random distribution of pitting, as shown in Fig.7. The pitting shape is defined as the cylinder, as shown in Fig.8.

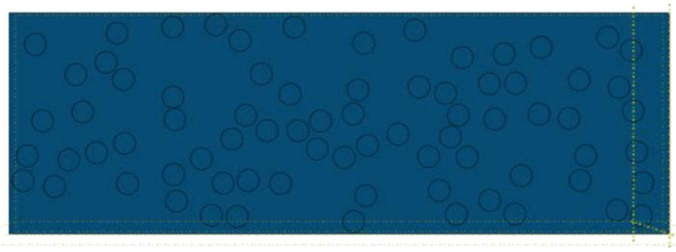

Fig. 7 Random distribution of pitting

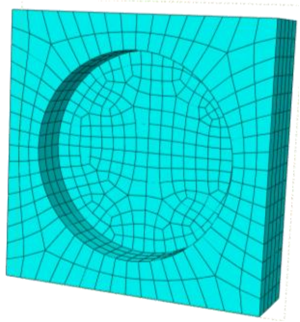

Fig. 8 Pitting shape

4.2. Test model parameter setting

To facilitate the finite element calculation, the variation in corrosion volume is achieved by adjusting the pitting depth. The corrosion volume *DOV* and pitting number *n* are used as the parameters to establish a finite element model of different pitting numbers. Corrosion volume *DOV* is defined as follows:

$$DOV = \frac{1}{V}\sum_{i=1}^{n} A_i \times h_i \tag{3}$$

Where V is the volume of the intact steel tube; N is the total number of pitting; A_i is the area of the *ith* pitting; h_i is the depth of the *ith* pitting.

In the square CFST column, the steel tube is Q345, concrete is C60, section size D is 200mm×200mm, column length L is 600mm, and steel tube thickness t is 4mm.The specimen parameters are shown in Table 1.

In Table 1, *I* is the intact specimen, *Re* is the pitting is regular arrangement, and *Ra* is the pitting is randomly generated. *n* is the total number of pitting, *R* is the radius of the pitting, *h* is the depth, *V* is the corrosion volume and *e* is the eccentric distance. Table 2 presents the ultimate bearing capacities of each specimen. P_{Re} represents the ultimate bearing capacity of the specimen experiencing regular pitting corrosion, while P_{Ra} denotes that of the specimen affected by random pitting corrosion.

Table 1
Test specimen parameters

	number	*n*	*R* (mm)	*h* (mm)	*DOV (%)*	*e* (mm)
I	0	/	/	/	/	20
Re /Ra	205	100	17.3	1/2/3/4	5/10/15/20	20
	405	200	12.2			
	605	300	10			
	805	400	8.65			

Table 2
Bearing capacity of various specimens under the influence of pitting

Number	Etching pit number	Volume loss rate	P_{Re}/kN	P_{Ra}/kN
I -0	/	/	2267.3	2267.3
Re -205-1	100	5%	2187.0	2179.0
Re -405-1	200		2211.5	2181.1
Re -605-1	300		2215.4	2183 0
Re -505-1	400		2216.6	2186.5
Re -205-2	100	10%	2137.8	2121.3
Re -405-2	200		2178.3	2144.5
Re -605-2	300		2186.7	2160.5
Re -505-2	400		2192.0	2163.6
Re -205-3	100	15%	2057.8	2038.7
Re -405-3	200		2143.4	2083.5
Re -605-3	300		2162.1	2122.9
Re -505-3	400		2167.4	2123.8
Re -205-4	100	20%	1625.1	1721.3
Re -405-4	200		1838.5	1726.3
Re -605-4	300		1908.5	1760.8
Re -505-4	400		1933.5	1804.7

5. Analysis of regular and random pitting

5.1. Load-deflection curve

Fig.9 presents the load-deflection curves for specimens with different regular and random pitting. For the specimens with regular pitting, corresponding to volume losses of 5%, 10%, 15%, and 20%, respectively. As corrosion progresses, the bearing capacity of the specimen decreases. Ultimate load of the specimens named Re-205 decreases obviously. When the corrosion is 5%, 10%, 15% and 20%, the bearing capacity decreases 60.8kN, 110.0kN, 190.0kN and 622.7kN, respectively. The results indicate that specimen's ultimate bearing capacity gradually deteriorates with increasing corrosion.

Notably, when the corrosion level reaches 20%, the bearing capacity degradation is 165% relative to that at a 15% corrosion level. This is because as the steel tube's volume loss rises, its outer cross-sectional area shrinks, reducing confinement on concrete and thus lowering the ultimate bearing capacity. Compared with regular pitting, the degradation of bearing capacity caused by random pitting will be more obvious than regular pitting with the same pitting number and corrosion rate. With the escalation of corrosion degree, the specimen's bearing capacity decline becomes more pronounced, especially when the corrosion level attains 20%. When the corrosion increased from 5% to 15%, the maximum ultimate load increment can be increased from7.5kN to 85.1kN. However, once the quantity of corrosion pits surpasses 300, the bearing capacity of the specimen remains largely unaffected. For example, when the pitting increases from 300 to 400, the maximum ultimate load change of the specimen is about 3.5kN.When the volume loss reaches 20%, no matter the specimens are under regular pitting or random pitting, the corrosion pit penetrates the steel tube, resulting in the weakest confinement of the steel tube on the concrete and a sudden drop in the bearing capacity.

However, under the same corrosion condition, specimen's ultimate bearing capacity under regular pitting varies with the number of pitting sites.Take the Re205 for example, when the corrosion is 5%, The maximum load carrying capacity of Re405, Re605 and Re805 increases by 24.5kN, 28.4kN and 29.6kN, respectively; When the corrosion is 10%, The ultimate bearing capacity of Re405, Re605 and Re805 increases by 40.5kN, 48.9kN and 54.2kN, respectively; When the corrosion is 15%, The ultimate bearing capacity of Re405, Re605 and Re805 increases by 80.6kN, 104.3kN and 109.6kN, respectively; When the corrosion is 20%, the ultimate bearing capacity of Re405, Re605 and Re805 increases by 213.4kN, 283.8kN and 308.4kN, respectively. This is due to the same volume corrosion, the area of single pit such as Re405, Re605 and Re805 decreases compared with Re205 in the compression area of middle section, and the constraint effect on concrete gradually increases. Consequently, it will result in an elevation of the bearing capacity. Under a constant corrosion condition, the impact of an increasing number of pitting sites on the bearing capacity will gradually diminish. When the number of pitting sites reaches 300, the variation in pitting begins to affect the stability of the specimen's bearing capacity. Take Re605 and Re805 for example, the ultimate load at each corrosion is extremely close, and the maximum difference is about 25.4kN. This is because when the number of corrosion pits gradually increases to 300, the corrosion's impact on the bearing capacity is closer to uniform corrosion. Specimen's load-carrying capacity with random pitting is significantly lower than that of specimen with regular pitting. The bearing capacity of Ra405, Re605 and Re805 is 112kN, 148kN and 120kN larger than that of Ra205, Ra405 and Ra605. However, when the pitting is 100, the bearing capacity of Re205 will be lower than that of Ra205. This may be related to the distribution of pitting. Compared with Ra205, the pitting of Re205 is near the middle part, and the reduction of cross-section area of the steel tube is more obvious, resulting in the weaker constraint of tube on the concrete.

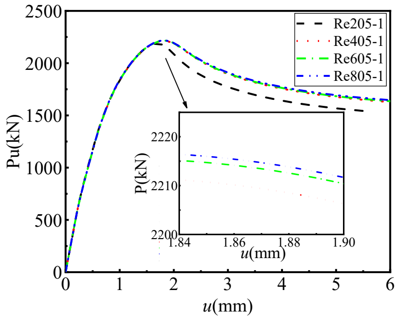

Regular pitting

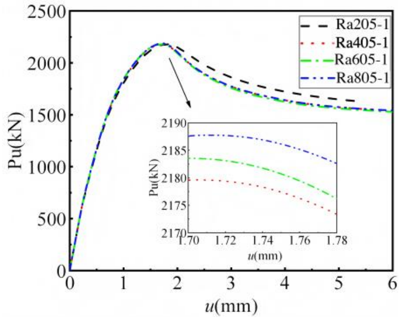

Random pitting

(a) DOV =*5%*

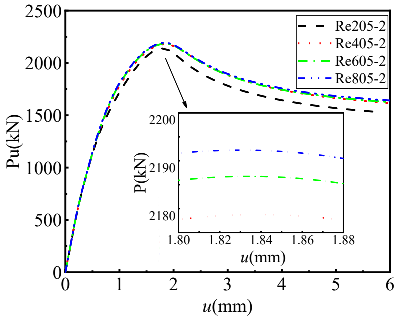

Regular pitting

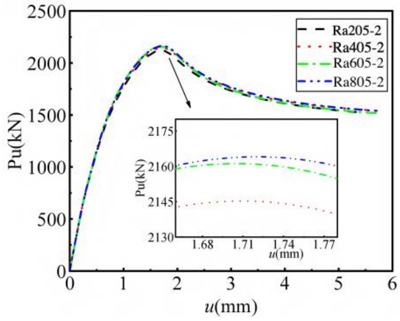

Random pitting

(b) DOV =10%

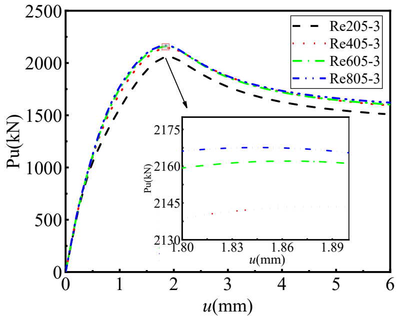

Regular pitting

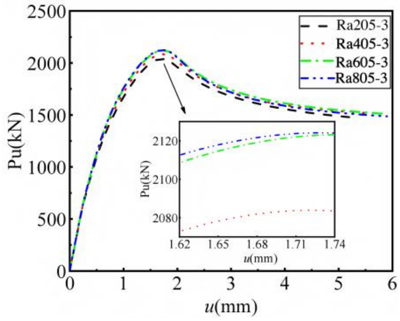

Random pitting

(c) DOV =15%

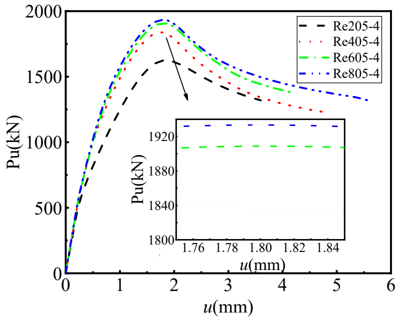

Regular pitting

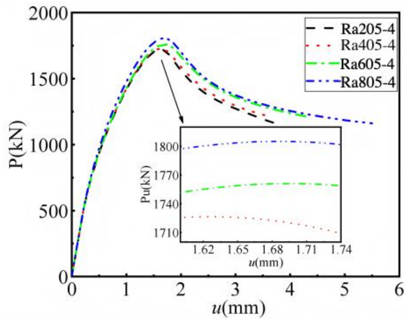

Random pitting

(d) DOV =20%

Fig. 9 Load-displacement of different DOV

5.2. Stress distribution

Fig.10 illustrates the stress-vertical displacement correlation for the steel tube It shows that the pitting volume loss exerts a negligible impact on the Mises stress of the steel tube. For regular pitting, the development of transverse stress and longitudinal stress under the same pitting will be slightly different with the increase of corrosion. As the tube attains its yield strength, the longitudinal stress in the middle section progressively diminishes with escalating corrosion. This can be ascribed to the fact that the increasing corrosion gradually degrades the steel tube's strength, consequently leading to a reduction in its longitudinal stress. The transverse stress of the steel tube progressively decreases with the increase in corrosion, which is due to the weakening of concrete constraint by steel tube caused by pitting. At the same time, the increase of pitting will also cause the early yield of steel tube, which the most obvious is Re205. When the corrosion is 5%, the displacement is 0.97mm when the steel tube yielded, while the corrosion is 10% and 15%, the displacement is 0.94mm and 0.85mm, decreasing by 3% and 12.4%, respectively.

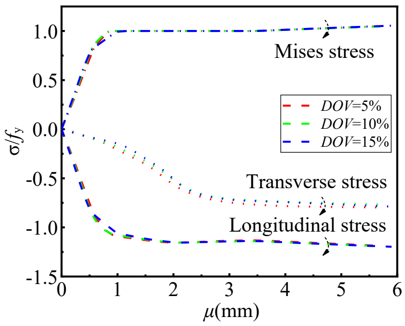

(a) Re205

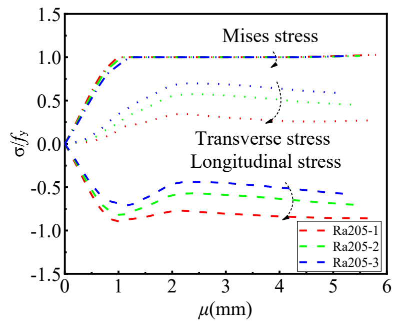

(b) Ra205

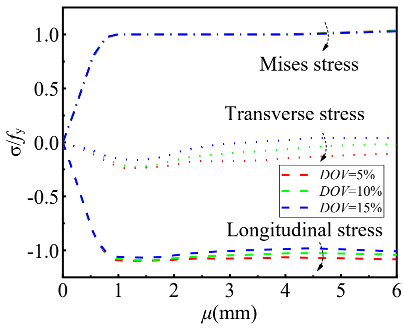

(c) Re405

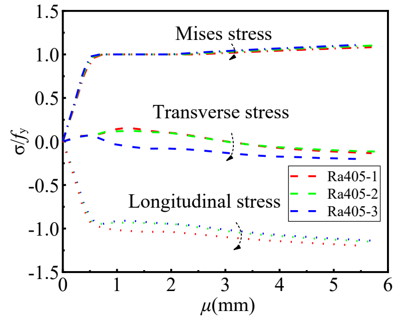

(d) Ra405

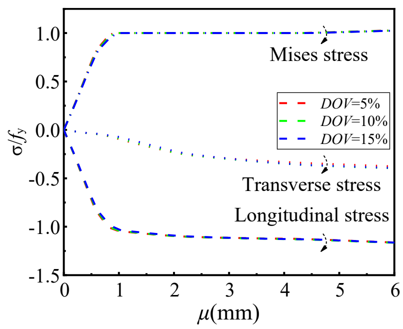

(e) Re605

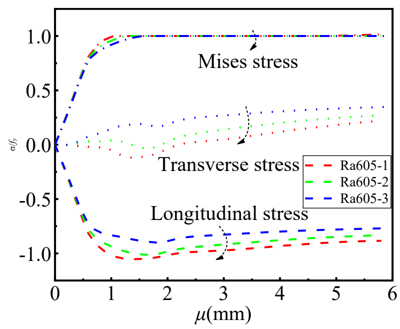

(f) Ra605

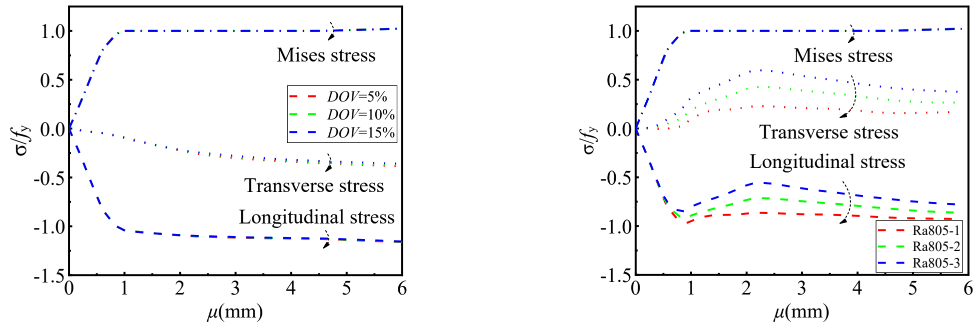

(g) Re805 (h) Ra805

Fig. 10 Longitudinal stress-vertical displacement curve of steel tube

For random pitting, pitting volume loss significantly affects steel tube's longitudinal and transverse stresses. When the pitting ratio rises from 5% to 15%, the longitudinal stress decreases as the pitting ratio increases. The longitudinal stress of Ra205, Ra405, Ra605, and Ra805 ranged from $0.88f_y$, $0.97f_y$, $1.04f_y$, $0.94f_y$ to $0.67f_y$, $0.93f_y$, $0.90f_y$, $0.78f_y$, by about 24%, 4%, 13.5% and 17%, respectively. The transverse stress in the steel tube progressively rises as the corrosion degree increases, which is due to the increase of pitting, which strengthens the contact between the corrosion pit and concrete, leading in the increase of transverse stress. The increase of pitting will also cause the advance yield of steel tube. Compared with regular pitting, random pitting will be more obvious than regular pitting. Take Ra205 for example, the displacement of the specimen with the corrosion of 5% is 0.63mm when the steel cylindrical conduit is yielded, and the displacement of the specimen with the corrosion of 10% and 15% is 0.58mm and 0.55mm, reducing 8% and 12.7%, respectively.

Fig.11 illustrates the stress-vertical displacement relationship of concrete in the middle section. It's evident that concrete's transverse stress rises with increasing corrosion. This is attributable to the enhanced contact between the steel tube and concrete induced by the increase in pitting. Additionally, the longitudinal stress of concrete also increases as corrosion intensifies. For regular pitting, take the Re205 with 100 corrosion pits for example, concrete's longitudinal stress in the limit state with 5% of corrosion is 1.13 f_c', Whereas the concrete's longitudinal stress with 10% and 15% corrosion is 1.41 f_c', 1.71 f_c', increasing by 24.8% and 51.3%, respectively. Owing to the proliferation of pitting, the load-bearing capacity of the steel tube progressively diminishes, while the load borne by the concrete gradually rises, consequently leading to an increase in the longitudinal stress of the concrete. Simultaneously, the presence of pitting induces an uneven longitudinal stress distribution in the middle section concrete, inducing stress concentration and thereby elevating the longitudinal stress of the concrete. Additionally, the evolution of corrosion pits also influences the stress development of the concrete. At the same corrosion, the longitudinal stress of concrete will change with the change of the pitting. This is due to the increase of the pitting, which increases the effective constraint of the concrete at the middle section. At the same time, With the increase of the pitting, the pitting will be uniform at middle section, and the stress concentration will be significantly weakened.

For random pitting, take Ra205 for example, the axial-direction stress within concrete in the limit state with corrosion of 5% is $1.28f_c'$, and the longitudinal stress of concrete with corrosion of 10% and 15% of the specimens is $1.42f_c'$, $1.58f_c'$, increasing by 11.2% and 23.4%, respectively. The increase of longitudinal stress of concrete under random pitting is similar to that of regular pitting, which is caused by the increase loading of concrete caused by the change of pitting, and the constraint of surrounding pitting on concrete is uneven, resulting in the stress concentration. However, different from the regular pitting, the longitudinal stress of concrete in the middle section is not much different under the same corrosion, which indicates that the change of pitting will not lead to the obvious change of the stress along the axial direction in concrete in the middle section under the random pitting.

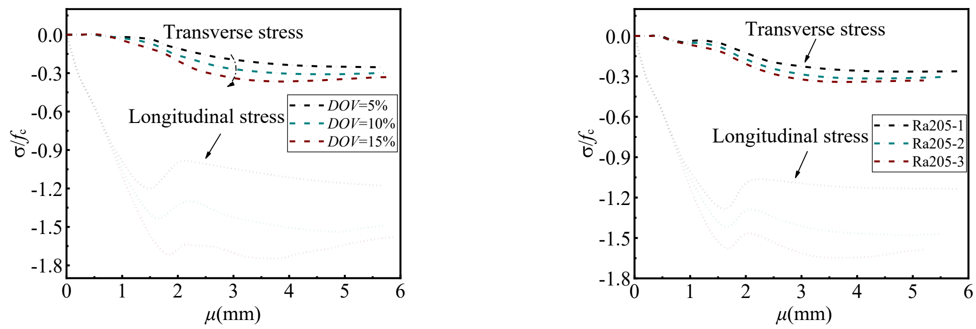

(a) Re205 (b) Ra205

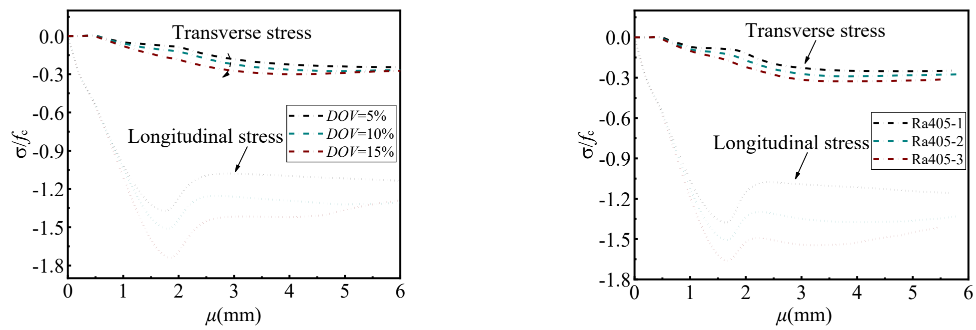

(c) Re405 (d) Ra405

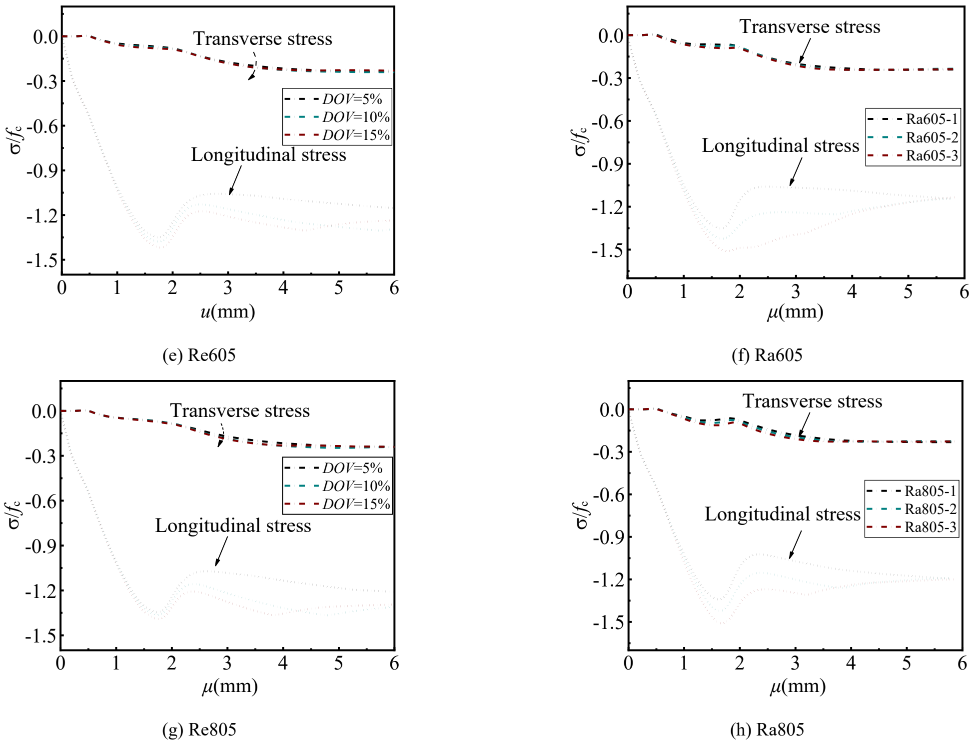

Fig. 11 Longitudinal stress-vertical displacement curve of concrete in middle section

5.3. Interaction

Fig12 illustrates the relationship between vertical displacement and contact stress for the steel tube-concrete interface. It shows that the contact stress is closely related to the corrosion degree and has the same change rule. During the initial loading phase, the contact stress at the steel-concrete interface is zero, implying no contact between the two. This stems from steel's higher Poisson's ratio than concrete's at the initial loading stage, leading to greater transverse deformation in steel relative to concrete, which results in the absence of contact between them. As the loading escalates, concrete's transverse deformation exceeds steel's, facilitating their contact. Regular pitting and random pitting trigger local steel buckling, prompting early steel-concrete contact, and will change with the change of corrosion. When the corrosion is 5%, the tube will contact with the concrete when the vertical displacement of the specimen with the pitting number of 100 reaches 0.31mm and 0.29, respectively, 6.5% compared with regular pitting. And the corrosion is 10% and 15%, the vertical displacement decreases by 6% and 10%, 5.1% and 8.4%, respectively. Moreover, the progression of pitting corrosion will diminish the contact at the steel-concrete interface. When the corrosion is 5%, the contact stress in the limit state is about 8.9MPa and 9.75MPa, respectively, 0.85MPa increment than regular pitting. When the corrosion increases to 10% and 15%, the contact stress decreases to 6.92MPa and 5.43MPa, 8.37MPa and 6.66MPa, respectively. For regular pitting, the change of pits also has an impact on the contact stress. When the number of pits increases from 100 to 400, the contact stress increased from 8.9MPa to 10.49MPa, increasing by about 17.8%, that is the reason why the bearing capacity changes with the increase of the number of pitting. For random pitting, when the number of pitting is 300, the contact stress at the middle section is 11.3MPa, which is significantly greater than the contact stress of other number of pitting. This may be related to the distribution of pits under the random distribution. When the number of pitting is 300, there is no distribution of pitting near the value point, so the contact stress at this point is higher than that under the other number of pits.

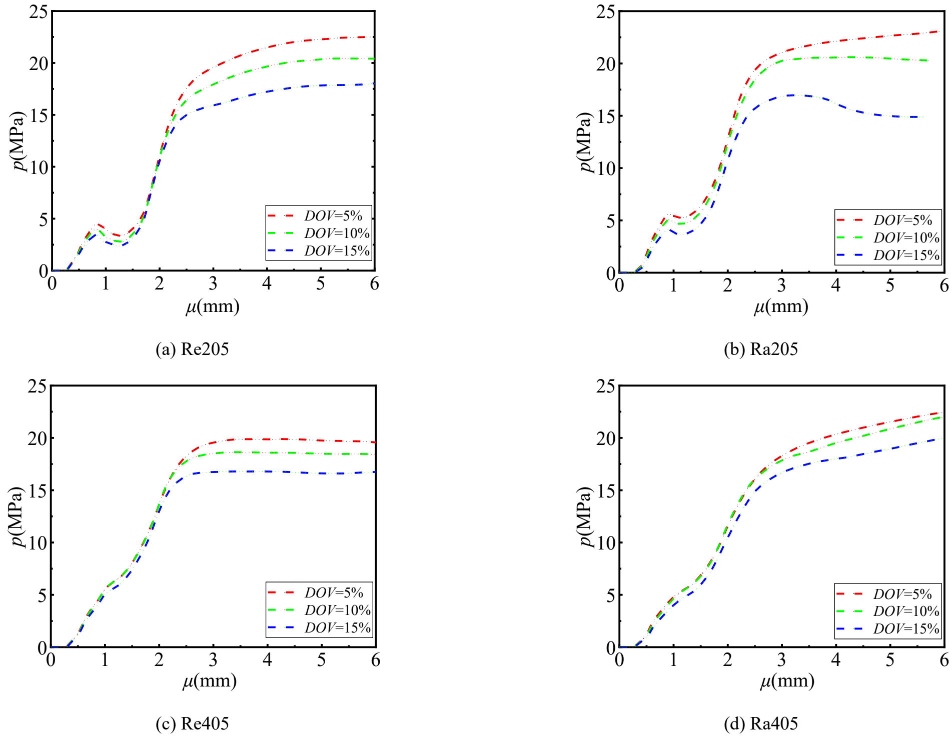

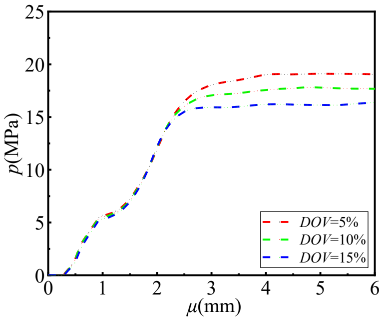

(e) Re605

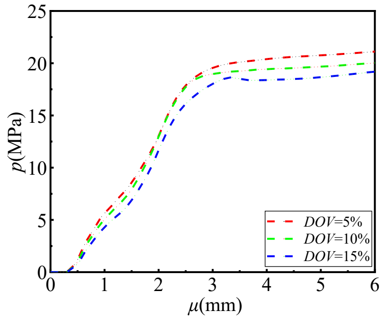

(f) Ra605

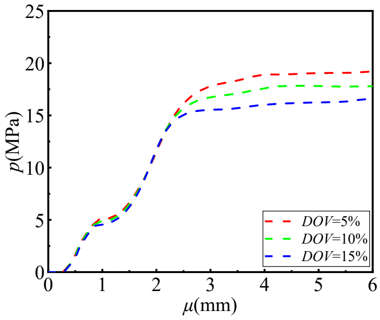

(g) Re805

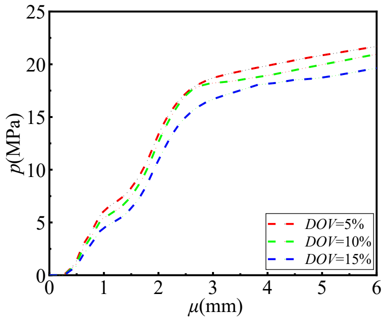

(h) Ra805

Fig. 12 Mid-section corner contact stress

6. The influence on different parameters

6.1. Eccentricity

Fig.13 presents the load-deflection curve for various eccentricities. It shows that maximum load will decrease with the increment of eccentricity. When the eccentricity increases from 0.25 to 1, maximum load of Re205-1 with regular pitting will decrease from 2187kN to 996kN, decreasing by 54.5%. When the eccentricity increases from 0.25 to 0.5, maximum load will decrease by 23.3%; when the eccentricity increases from 0.5 to 0.75, maximum load will decrease by 21.6%; when the eccentricity increases from 0.75 to 1, maximum load will decrease by 19.4%. However, maximum load of Ra205-1 under random pitting is consistent with the regular pitting. When the eccentricity increases from 0.25 to 1, the decrease ratio of maximum load is about 20.9%, 21.4% and 19%, respectively.

6.2. Concrete strength

Fig.14 illustrates the load-deflection curves for varying concrete strengths. It indicates that both the ultimate load and stiffness increase as the concrete strength rises. When the concrete's strength increases from C30 to C60, the ultimate load of Re205-1 with regular pitting will increase from 1556kN to 2186kN, an increase of 40.5%. When the strength of concrete rises from C30 to C40, the maximum load will increase by 13.8%; when concrete strength rises from C40 to C50, the ultimate load increases by 11.8%; when it rises from C50 to C60, the increase is 10.3%. However, the ultimate load of Ra205-1 under random pitting is consistent with the regular pitting. When the concrete strength rises from C30 to C60, the increase of the maximum load is about 14.0%, 14.1% and 13.9%, respectively. The ultimate load affected by random pitting is slightly lower than that of affected by regular pitting. For each grade of concrete, the increase of the bearing capacity under the two corrosion conditions is basically consistent.

6.3. Steel strength

Fig.15 presents the load-deflection curves for varying steel strengths. It indicates that the ultimate load will rise as the steel strength increases, while the initial stiffness remains largely unchanged. When the yield strength of steel increases from 235MPa to 460MPa, the maximum load of Re205-1 with regular pitting will increase from 1920kN to 2489kN, increasing by 29.3%. When steel's strength increases from 235MPa to 345MPa, the ultimate load will increase by 13.9%; when steel's strength increases from 345MPa to 420MPa, the ultimate load of the will increase by 9.3%; when steel's strength increases from 420MPa to 460MPa, the ultimate load will increase by 4.1%. However, the ultimate load of Ra205-1 under random pitting is consistent with the regular pitting When the steel strength increases from 235MPa to 460MPa, the increase ratio of the ultimate load is about 14.3%, 8.3% and 4.0%, respectively. The ultimate load of affected by random pitting is slightly lower than that of affected by regular pitting. For each increase of the steel, the increase of the bearing capacity under the two corrosion conditions is basically consistent.

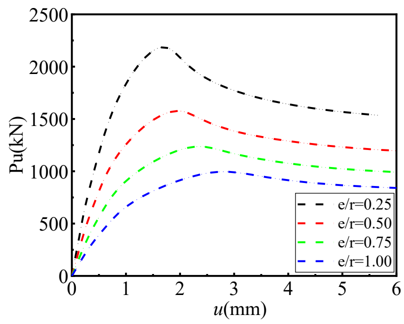

(a) Re205-1

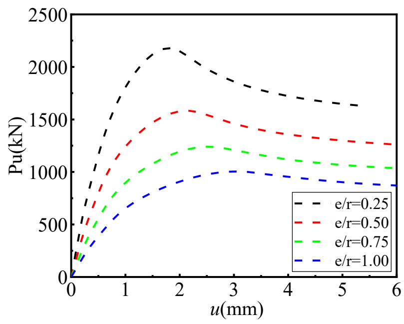

(b) Ra205-1

Fig. 13 Load-deflection of different eccentricities

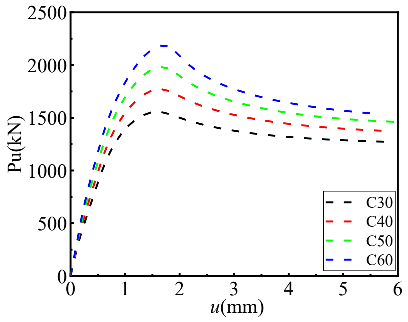

(a) Re205-1

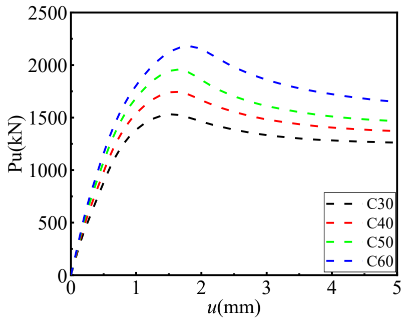

(b) Ra205-1

Fig. 14 Load-deflection of different concrete strengths

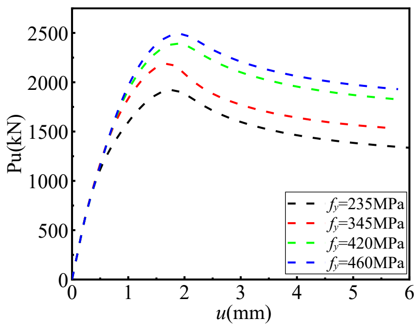

(a) Re205-1

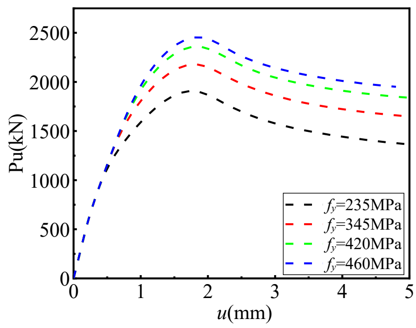

(b) Ra205-1

Fig. 15 Load-deflection of different steel strengths

6.4. Steel tube thicknesses

Fig.16 illustrates the load-deflection curves for varying steel tube thicknesses. It indicates that both the ultimate load and stiffness will rise as the steel tube thicknesses increase.When steel tube's thickness increases from 4mm to 7mm, the ultimate load of Re205-1 with of regular pitting will increase from 2187kN to 2750kN, increasing by 25.7%. When the steel tube's thickness increases from 4 mm to 5 mm, the ultimate load exhibits a 7.8% increase; when it increases from 5 mm to 6 mm, the ultimate load rises by 7.9%; and when the thickness goes up from 6 mm to 7 mm, the ultimate load shows a 7.3% increment. However, the ultimate load of Ra205-1 with random pitting is consistent with the regular pitting. When the thickness of the steel tube increases from 4mm to 7mm, the increase ratio of the ultimate load is about 7.5%, 7.6% and 7.0%, respectively. The maximum load affected by random pitting is slightly lower than that of affected by regular pitting. For each thickness of steel, the increase of the bearing capacity under the two corrosion conditions is basically consistent.

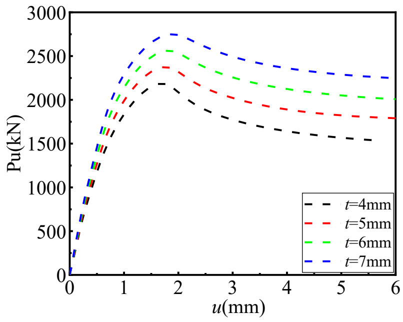

(a) Re205-1

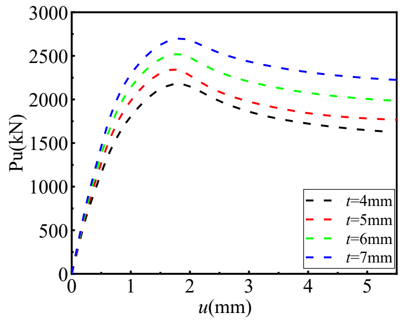

(b) Ra205-1

Fig. 16 Load-deflection of different steel tube thicknesses

7. Conclusions

This paper analyses the eccentric compression mechanical property of square CFST column with of regular and random pitting. And parametric analysis like eccentricity, concrete's compressive strength, steel strength and steel tube thicknesses is analyzed. The conclusions are as follows:

(1) Pitting reduces the specimen's maximum load bearing capacity. Specimens exhibiting regular pitting demonstrate a higher ultimate bearing capacity compared to those with random pitting. And under the same pitting, increasing pitting number will increase the bearing capacity, but when the pitting reach 300, the maximum bearing capacity of the specimen will remain stable.

(2) Pitting diminishes steel tube's strength, consequently resulting in a reduction of its longitudinal stress. Increased pitting enhances the steel-concrete interface interaction, raising transverse stress. It reduces the steel tube's load, increasing the concrete's load and thus elevating its longitudinal stress. At the same time, pitting will cause the steel tube to the yield state in advance, and with the increase of pitting, this situation will become more obvious.

(3) Pitting will cause the early contact between steel tube and concrete, Weakening the steel-concrete interaction, and cause the reduction of the bearing capacity of the specimen. The steel-concrete interaction gradually diminishes as pitting increases. However, under normal pitting conditions, a rise in pitting can enhance this interaction. But this influence rule is not applicable to random pitting.

(4) Under diverse parameters, specimens with regular pitting consistently exhibit higher load bearing capacity than those with random pitting. When the eccentricity increases from 0.25 to 0.5, 0.75, and 1.0, specimens' bearing

capacity with regular pitting will decrease by 23.3%, 44.9% and 64.5% respectively. However, specimens' bearing capacity with random pitting will decrease by 20.9%, 42.3% and 61.3%, respectively. When the strength of concrete increases from C30 to C40, C50 and C60, specimens' bearing capacity with regular pitting will increase by 13.8%, 25.6% and 35.9%, respectively, while the specimens with random pitting will increase by 14.3%, 22.6% and 26.6%, respectively. When the strength of the steel increases from 235MPa to 345MPa, 420MPa and 460MPa, specimens' bearing capacity with regular pitting will increase by 13.9%, 23% and 27.3%, respectively. Specimens' bearing capacity with random pitting will increase by 14.3%, 22.6% and 26.9%, respectively. When the thickness of the steel tube increases from 4mm to 5mm, 6mm and 7mm, specimens' bearing capacity with regular pitting will increase by about 7.8%, 15.7% and 23%, respectively. Specimens' bearing capacity with random pitting will increase by 7.5%, 15.1% and 22.1%, respectively.

Conflict of interest statement

The authors state no conflict of interest exists.

Data availability

The corresponding author can provide access to the data, models, and code that substantiate the outcomes of this work upon a fair request.

Funding

This work was supported by the open research fund of Shenyang Key Laboratory of low-carbon Transportation Construction, Maintenance and Operation (No.JT-Y24-5), 2024 Scientific research platform construction project of Liaoning Education Department (No.LJ232410153005) and Liaoning Provincial Department of Natural Science(No. 2022-MS-399) .

References

[1] Le L, Sofi M, Lumantarna E. The combined effect of stress and corrosion on mild steel[J]. Journal of Constructional Steel Research, 2021, 185：106805.

[2] Gathimba N, Kitane Y. Effect of surface roughness on tensile ductility of artificially corroded steel plates[J]. Journal of Constructional Steel Research, 2021, 176:106392.

[3] Zhao Z, Liang B, Liu H, et al. Influence of pitting corrosion on the bending capacity of thin-walled circular tubes[J]. Journal of the Brazilian Society of Mechanical Sciences and Engineering, 2018, 40（11）：548.

[4] Cai J, Pan J, Lu C, et al. Nonlinear analysis of circular concrete-filled steel tube columns under eccentric loading[J]. Magazine of Concrete Research, 2020, 72（6）:292﹣303.

[5] Yan J-B, Chen A, Zhu J-S. Behaviours of square UHPFRC-filled steel tubular stub columns under eccentric compression[J]. Thin-Walled Structures, 2021, 159：107222.

[6] Zhou J, Chen Z, Liu D, et al. Experimental and numerical investigations on eccentric compression behavior of square CFST columns with inner spiral stirrup[J]. Structures, 2023, 57：105196.

[7] Han L-H, Hou C, Wang Q-L. Square concrete filled steel tubular (CFST) members under loading and chloride corrosion: Experiments[J]. Journal of Constructional Steel Research, 2012, 71：11﹣25.

[8] Hua Y-X, Han L-H, Wang Q-L, et al. Behaviour of square CFST beam-columns under combined sustained load and corrosion: Experiments[J]. Thin-Walled Structures, 2019, 136：353﹣366.

[9] Guo L, Huang H, Jia C, et al. Axial behavior of square CFST with local corrosion simulated by artificial notch[J]. Journal of Constructional Steel Research, 2020, 174：106314.

[10] Li J, Jia C, Guo L. Eccentric performance of slender CFST with machining defects representing local corrosion[J]. Structures, 2023, 56：105037.

[11] Xie L, Chen M, Sun W, et al. Behaviour of concrete-filled steel tubular members under pure bending and acid rain attack: Test simulation[J]. Advances in Structural Engineering, 2018, 22（1）：240﹣253.

[12] Hua Y, Han L-H, Hou C. Behaviour of square CFST beam-columns under combined sustained load and corrosion: FEA modelling and analysis[J]. Journal of Constructional Steel Research, 2019，157：249-259.

[13] Zhang T, Lyu X, Liu H, et al. Axial performance degradation of squared CFST stubs in severe cold and acid rain area[J]. Construction and Building Materials, 2020, 262：120612.

[14] Ali R B, Islam M M, Begum M, et al. Behavior of concrete-filled steel tubular cold-formed built-up slender square columns under eccentric compression[J]. Innovative Infrastructure Solutions, 2021, 6（4）：189.

[15] Hui C, Li Y, Li K, et al. Experimental investigation and analysis on the axial compressive performance of recycled concrete-filled corroded steel tubular columns[J]. Archives of Civil and Mechanical Engineering, 2022, 22（2）：97.

[16] Wang K, Chen M, Zhang R, et al. Finite element simulation of load bearing capacity of circular CFST long columns with localized corrosion under eccentric load[J]. Structures, 2022, 43：1629﹣1642.

[17] Luo S, Chen M, Huang H, et al. Eccentric compression test and ultimate load strength analysis of circular CFST long column with local corrosion[J]. Structures, 2023, 56：104937.

[18] Rui Zhang. Study on the effect of local corrosion on the mechanical properties of concrete-filled circular steel tube compression-bending members[D]. Nanchang, East China Jiaotong University, 2022: 10-12 21-38.